SEMARAK ILMU PUBLISHING

CFD Letters

Journal homepage:
https://semarakilmu.com.my/journals/index.php/CFD_Letters/index
ISSN: 2180-1363

Hydrodynamic Performance Analysis of Camber Ratio Variations on B-series Propeller Types

Mahendra Indiaryanto[1], Ketut Suastika[1,*], Taufiq Arif Setyanto[2]

[1] Department of Naval Architecture, Institut Teknologi Sepuluh Nopember,Surabaya, 60111, Indonesia
[2] Research Center for Hydrodynamics Technology, National Research and Innovation Agency (BRIN), Surabaya 60117, Indonesia

ARTICLE INFO

Article history:
Received 14 September 2023
Received in revised form 17 October 2023
Accepted 18 November 2023
Available online 29 February 2024

Keywords:
B-Series; Camber; CFD; Efficiency; Polynomial; RANSE

ABSTRACT

The hydrodynamic performance of the B-series propeller can be determined by calculating the polynomial equation published by MARIN. Furthermore, analysis and evaluation of B-series propeller modifications can be done by varying the camber ratio of the foil. The camber ratio affects the lift force on the propeller foil, directly affecting the propeller thrust and torque. Numerical calculations were carried out using Computational Fluids Dynamics (CFD), based on Reynolds Averaged Navier Stokes Equations (RANSE) and turbulence model in the form of explicit algebraic stress models (EASM). The overall results of this study show an increase in efficiency of 4.182 on the foil with a camber ratio of 2.2% when compared to the foil camber ratio of 0%.

1. Introduction

Recently, many studies have been conducted to investigate ship propeller and wind turbine performance using numerical methods [1, 2]. The Reynolds Averaged Navier-Stokes Equation (RANSE) approach can be a practical alternative to conventional calculation methods using potential theory [3]. RANSE can describe the turbulent flow around a propeller more efficiently than calculating the turbulence directly. This approach allows for more efficient modeling of how the fluid flow interacts with the propeller under various conditions [4].

Calculations using RANSE cannot be separated from the turbulence modeling used. The turbulence model approach uses the Explicit Algebraic Stress Model (EASM). An efficient turbulence modeling is available in the literatures. This is because EASM provides better calculation efficiency and can overcome the limitations that usually occur in turbulent viscosity models [5].

In addition, other efforts have also been made to calculate propeller performance using CFD methods, but they rarely make changes to geometric parameters to improve propeller performance. For example, The study of the changes in thrust and cavitation values of the propeller was determined by changing the rake angle of the B-Series propeller. The simulation results show that the maximum thrust and efficiency values are generated at a rake angle change of 5°, while the

* *Corresponding author.*
E-mail address: k_suastika@na.its.ac.id (I Ketut Suastika)

https://doi.org/10.37934/cfdl.16.7.3953

smallest thrust value is obtained at a rake angle variation of 25° [6]. Numerical study such as increasing the efficiency of the propeller was also carried out by changing the pitch angle to improve the effect on the wake distribution [7]. A developed program using subroutin to optimize the B-series propeller performance was carried out [8]. The effort to increase the B-series propeller performance was also carried out by attaching cap fin and ducted [9]. The polynomial method was also applied to optimize the B3-611 (B-series propeller) performance by varying the diameter and P/D ratio[10].

The NACA 66 series foil type is used by the B-series propeller [11]. The study, which involved the changing camber ratio of NACA 66 series foil, still needs to be developed to improve the propeller performance. In this study, increasing the B-series propeller performance is done by changing the camber ratio, which is the ratio between camber and chord length, while maintaining the foil thickness ratio. The varying of camber ratio also includes the difference between the susction side and pressure side of the propeller geometry.

2. Methodology

In this study, the effort to improve the propeller's performance was carried out by varying the propeller camber ratio of the B-series propeller B4-40. This type of propeller was used for the propulsion test of the mini LNG (Liquified Natural Gas) ship model. To understand the impact of these modifications in greater depth, the research involved numerical simulations using CFD methods to analyze the thrust coefficient (K_T), torque coefficient (K_Q), and efficiency (η) of the propeller.

By using CFD simulation calculations, this study aims to provide a more comprehensive insight into the performance of the B4-40 propeller with modified camber ratio. The results of this study are expected to provide valuable contributions to developing more efficient and effective mini LNG ship propeller technology.

2.1 Governing Equations

To numerically describe turbulent flow around a propeller model, partial differential equations are required to describe fluid flow behavior in space and time. In computational fluid dynamics and propeller analysis, the Navier-Stokes equations are used to model fluid flow in turbulent conditions. The aim is to understand how the propeller interacts with the surrounding fluid flow and how its performance can be improved.

RANSE, which calculated the variable of flow velocity, pressure, and vorticity distribution around the propeller [12], is discribe as follows,

$$\frac{\partial u_i}{\partial x_i} = 0 \tag{1}$$

$$\frac{\partial u_i}{\partial t} + \frac{\partial u_i u_j}{\partial x_i} = -\frac{1}{\rho}\frac{\partial P}{\partial x_i} + \frac{\partial}{\partial x_j}\left(\mu \frac{\partial u_i}{\partial x_j}\right) + \frac{\partial}{\partial x_i}\left(\mu \frac{\partial u_i}{\partial x_j}\right) - \frac{\partial}{\partial x_j}\left(-\rho \overline{u_i' u_j'}\right) \tag{2}$$

where ρ is the density of the fluid, u_i is the average component of the flow velocity in the x_i direction; x_i is the space coordinate in the i direction, μ is the dynamic viscosity, $\dot{u}_i$ is the fluctuation of the flow velocity in the i direction, *p* is the pressure and *t* is the time.

The advection and diffusion are factors affecting the change in fluid flow velocity in the equation , which play an important role in the change in velocity distribution over time. Advection represents the changes caused by the movement of the fluid flow itself. $\frac{\partial}{\partial x_j}\left(\mu \frac{\partial u_i}{\partial x_j}\right) + \frac{\partial}{\partial x_i}\left(\mu \frac{\partial u_i}{\partial x_j}\right)$ is the

combination of advection and diffusion that provides a comprehensive picture of how the velocity distribution and other fluid flow properties can change over time. The equation $-\frac{\partial P}{\partial x_j}$ reflects the impact of pressure difference in the flow on velocity change [12].

The selection of an appropriate turbulence model is key in RANSE simulations. The term $\left(-\rho\overline{u_i'u_j'}\right)$ is the Reynold stress, which in this numerical simulation is defined as the EASM (Explicit Algebraic Stress Models) turbulent flow equation [3]. The boundary conditions for the EASM modeling equation are the same as those described in the "Wilcox Two-Equation Model" section. The Reynolds stress is modeled in the form of eddy viscosity as follows [13],

$$\tau_{ij} = 2\mu_t S_{ij} - \frac{2}{3}\rho K\delta_{ij} \tag{3}$$

where τ_{ij} is the component of the Reynolds stress tensor that reflects the momentum transfer between directions i and j, S_{ij} is the mean deformation rate tensor, which describes the mean deformation of the flow. The parameter μ_t is the turbulent viscosity (Eddy Viscous), which describes the impact of turbulence on the mean flow with the equation,

$$\mu_t = \frac{\rho K}{\omega} \tag{4}$$

2.2 Geometrical Modeling

The B-series propeller model with a scale of 1:8.333 from the full-scale propeller, as shown in Table 1, was used as the basis for modifing the camber ratio. The main purpose is to reduce the number of grid elements or cells in CFD simulations and shorten the time required for computation [9]. Thus, the scaling of the model help to overcome computational resources limitations.

Table 1
Main dimension of propeller

Type	Unit	B-Series	
		Model	Prototype
Dimension (D)	mm	180	1500
The number of blades	-	4	4
Expanded area ratio (Ae/Ao)	-	0.4	0.4
Pitch of ratio	-	1.144	1.144
Rotation propeller	Rpm	750	260

Modifications to the B4-40 propeller were made by changing the camber ratio of the B-series propeller foils (see Figure 1). This technique has been widely studied in the field of aeronautical engineering, where the meanline curvature of the foil creates asymmetry between the two working surfaces of the airfoil, namely the upper and lower surfaces. The concept is based on Wing Section Theory, where the camber is usually engineered into the foil to maximize the lift coefficient value [14]. A foil is considered to have a positive camber when the propeller's top surface is more convex than its bottom surface. The purpose of this modification is to improve propeller performance.

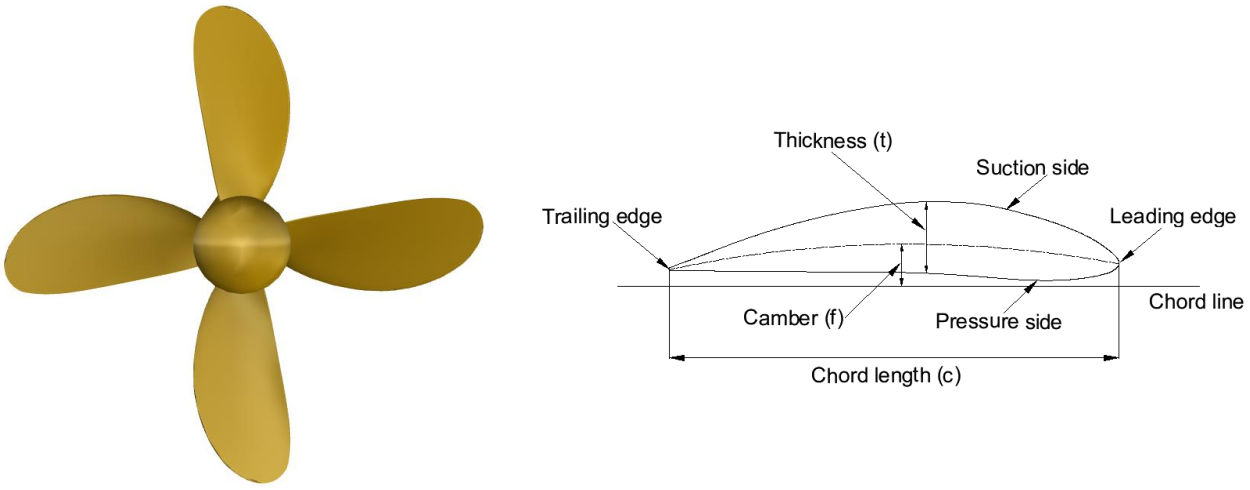

(a) (b)

Fig. 1. (a) Model propeller B-series B4-40 and (b) Foil propeller B4-40 with camber

The camber ratio is the ratio between the camber (f) at the maximum thickness and the chord length (c) of the propeller blade profile. The camber ratio of 0% to 6% is a common range for NACA airfoils [15]. The camber ratio value of 0%, 1.6%, 2.2 % and 2,8%, as shown in Table 2. The simulation was carried out.

Table 2
Variation of camber ratio foil propeller B-Series

Camber Ratio (f/c)	0%	1.6%	2.2%	2.8%

The propeller performance diagram generated through the B-series propeller polynomial calculation is used as the basis to verify the CFD simulation results with a 0% camber ratio. The difference between the polynomial calculations and the CFD simulation results ensures that the CFD model provides results that match the existing polynomial approximations.

2.3 Computational Domain and Boundary Conditions

The domain, as shown in Figure 2, used in this simulation refers to the guidelines provided by ITTC (Internasional Towing Tank Conference) [16], which is expressed as a multiplication of the propeller diameter (D). The propeller center is 2D from the inlet, while the outlet distance is placed six times from the center of the propeller (6D). Meanwhile, the cylinder side boundaries are placed at least six times from the center of the propeller. The existence of boundary conditions far from the propeller center is important to avoid the effects of changes in flow due to propeller rotation. With a propeller diameter of 180 mm, the detailed image of the boundary conditions can be seen in Figure 2.

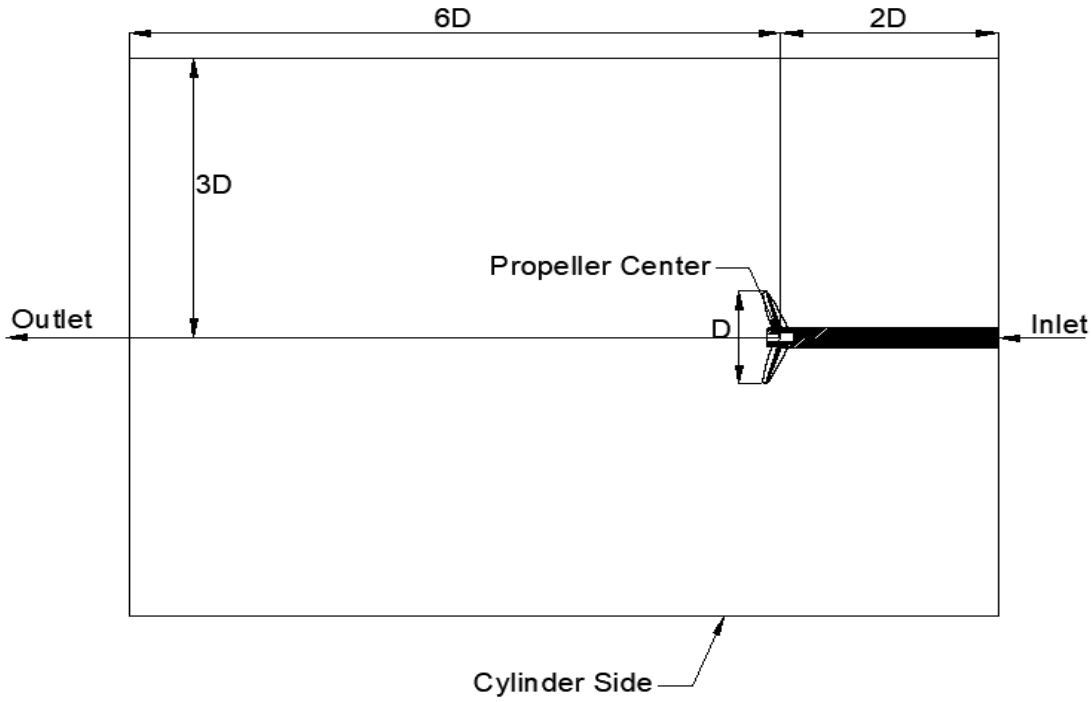

Fig. 2. Computational domain for the CFD simulations showing inlet, outlet and cylinder side

The boundary conditions for the simulation are as follows

i. The propeller shaft is set to a slip condition, where the shear stress component parallel to the wall surface must be zero, and the velocity component in the direction parallel to the wall surface must be present.
ii. On the propeller blades' surface, the boundary condition is set to wall function
iii. The boundary condition is set at the inlet as fixed velocity and zero pressure gradient.
iv. At the cylinder side, the boundary condition is set as fixed velocity and zero pressure gradient on the lateral face.
v. At the oulet side, the boundary condition is set as pressure is kept constant and equal to 0 during the computation.

2.4 Grid Generation and Grid Independence Test

The main purpose of meshing is to transform the continuous domain into a discrete form so that the Navier-Stokes flow equations can solve the calculations on each element. In the context of propeller analysis with CFD, meshing plays an important role because the mesh's quality and fit will affect the numerical solution's accuracy and convergence [17]. For this reason, the selection of the meshing arrangement in Figure 3 is illustrated by increasing the number of grids in the area close to the propeller and making them loose in the area far from the propeller. This method proved to be effective in saving time during CFD simulation.

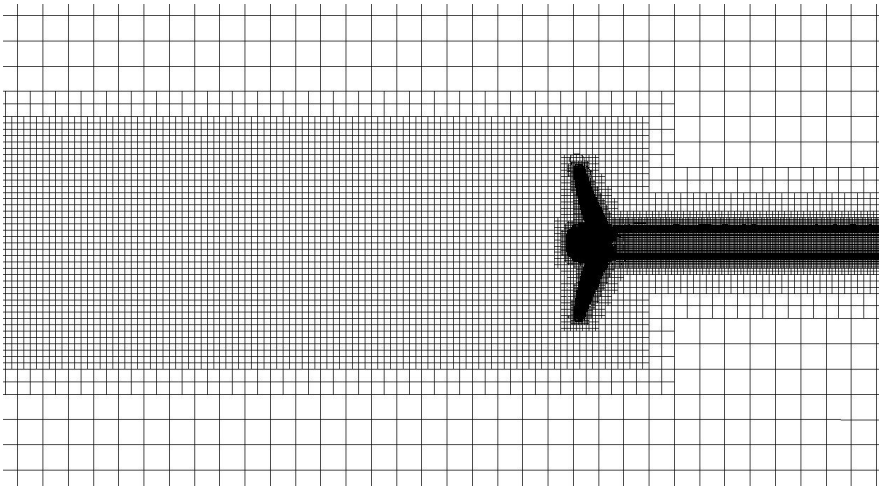

Fig. 3. Meshing model propeller B4-40

In this simulation, the variable to be known is the thrust value of the 3D propeller model in the open water simulation. Furthermore, the thrust value is converted into a propeller thrust coefficient. The value is compared with the number of cells, approximately two times the previous simulation. If the difference in the resulting thrust coefficient value is less than 2% (two percent), then the number of cells is considered good [18]. This study uses a difference in thrust coefficient value of less than 1% during simulation (see Table 3 and Figure 4).

Table 3
Grid independence propeller of B4-40

Number of element	421,048	777,305	1,349,593	2,394,333
K_T	0.4027	0.3947	0.3906	0.3868
Percentage	-	2.039%	1.030%	0.996%

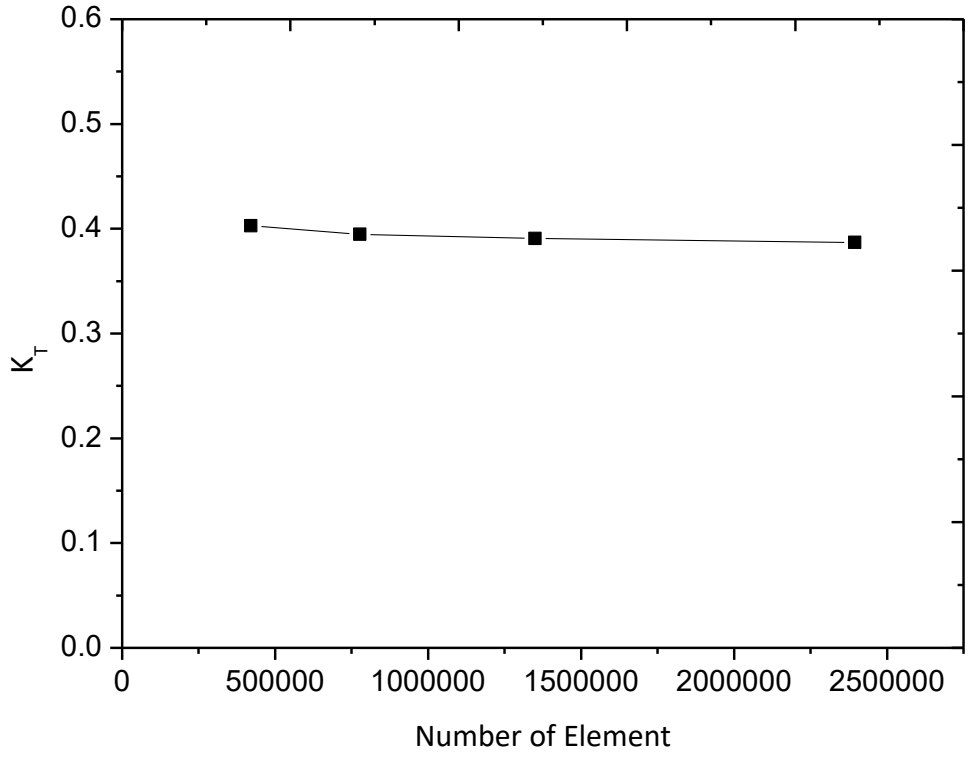

Fig. 4. Grid independence simulation of CFD propeller B4-40 for K_T

3. Verification of the CFD Results

Comparing the data obtained from computational fluid dynamics simulations with the calculated results of a polynomial model of a B-series propeller allows us to measure the precision and accuracy of the simulations.

3.1 Polynomial Propeller B-series

The performance of the B-series propeller diagram can be known by using the B-series propeller polynomial equation so that the results obtained from the equation are the thrust coefficient (K_T), torque coefficient (K_Q), and propeller efficiency (η) [19]. Before calculating the B series propeller polynomial, it is necessary to calculate the propeller Reynolds. Refering to the ITTC -Recommended Procedures and Guidelines 2014, Revision 3 [20], the Reynold number was calculated at r/R 0.7 using the following equation:

$$Re_{0.7} = \frac{C_{0.7}\sqrt{V_a^2 + (0.7\pi nD)}}{v} \tag{5}$$

if the value of Re < 2 x 10^6, then the calculation of K_T and K_Q based on the following equation is used:

$$K_T = \sum_{n=1}^{39} C_n^T \ (J)^{s_n}.(P/D)^{t_n}.(A_E/A_O)^{u_n}.(Z)^{v_n} \tag{6}$$

$$K_Q = \sum_{n=1}^{47} C_n^Q \ (J)^{s_n}.(P/D)^{t_n}.(A_E/A_O)^{u_n}.(Z)^{v_n} \tag{7}$$

Where C is the propeller chord length, Va is the Velocity Advance, n is the propeller rotation, D is the propeller diameter, J is the advance coefficient, P/D is the pitch and diameter ratio, A_E/A_O is the propeller area ratio, and Z is the number of propellers. Meanwhile, the values of s, t, u, and v are the regression coefficient and exponent values of K_T and K_Q, which can be seen in Tables 1 and 2.

If the values 2 x 10^6 < Re < 2 x 10^9 need to be added, corrections in the form of ΔK_T and ΔK_Q with the following equations (see Table 4 and 5):

$$\begin{aligned}\Delta K_T = {} & 0.000353485 \\ & -0.00333758\ (\mathrm{A}_E/\mathrm{A}_O)\mathrm{J}^2 \\ & -0.00478125(\mathrm{A}_E/\mathrm{A}_O)\ (\mathrm{P/D})\mathrm{J} \\ & +0.000257792(\log R_n - 0.301)^2\ (\mathrm{A}_E/\mathrm{A}_O)\mathrm{J}^2 \\ & +0.0000643192(\log R_n - 0.301)\ (\mathrm{P/D})^6\mathrm{J}^2 \\ & -0.0000110636(\log R_n - 0.301)^2\ (\mathrm{P/D})^6\mathrm{J}^2 \\ & -0.0000276305(\log R_n - 0.301)Z\ (\mathrm{A}_E/\mathrm{A}_O)\mathrm{J}^2 \\ & +0.0000954(\log R_n - 0.301)Z\ (\mathrm{A}_E/\mathrm{A}_O)\ (\mathrm{P/D})\mathrm{J} \\ & +0.0000032049(\log R_n - 0.301)Z^2\ (\mathrm{A}_E/\mathrm{A}_O)\ (\mathrm{P/D})^3\mathrm{J}\end{aligned} \tag{8}$$

$$\begin{aligned}\Delta K_Q = & -0.000591412 \\ & +0.00696898(\mathrm{P/D}) \\ & -0.0000666654\,\mathrm{Z}\,(\mathrm{P/D})^6 \\ & +0.0160818(\mathrm{A}_E/\mathrm{A}_O)^2 \\ & -0.000938091(\log R_n - 0.301)\,(\mathrm{P/D}) \\ & -0.00059593(\log R_n - 0.301)\,(\mathrm{P/D})^2 \\ & +0.0000782099(\log R_n - 0.301)^2\,(\mathrm{P/D})^2 \\ & +0.0000052199(\log R_n - 0.301)\,Z\,(\mathrm{A}_E/\mathrm{A}_O)^2 \\ & -0.00000088528(\log R_n - 0.301)^2 Z\,(\mathrm{A}_E/\mathrm{A}_O)\,(\mathrm{P/D})\mathrm{J} \\ & +0.0000230171(\log R_n - 0.301) Z\,(\mathrm{P/D})^6 \\ & -0.00000184341(\log R_n - 0.301)^2 Z\,(\mathrm{P/D})^6 \\ & -0.00400252(\log R_n - 0.301)\,(\mathrm{A}_E/\mathrm{A}_O)^2 \\ & -0.000220915(logR_n - 0.301)^2(A_E/A_O)^2\end{aligned} \tag{9}$$

$$\begin{Bmatrix}K_T \\ K_Q\end{Bmatrix} = \begin{Bmatrix}K_T(R_n = 2x10^6) \\ K_Q(R_n = 2x10^6)\end{Bmatrix} + \begin{Bmatrix}\Delta K_T \\ \Delta K_Q\end{Bmatrix} \tag{10}$$

Table 4
Regression coefficient and exponent K_T

K_T	C	s	t	u	v	K_T	C	s	t	u	v
		J	P/D	A_E/A_O	Z			J	P/D	A_E/A_O	Z
1	0.000880496	0	0	0	0	21	0.010465	1	6	2	0
2	-0.204554	1	0	0	0	22	-0.00648272	2	6	2	0
3	0.166351	0	1	0	0	23	-0.00841728	0	3	0	1
4	0.158114	0	2	0	0	24	0.0168424	1	3	0	1
5	-0.147581	2	0	1	0	25	-0.00102296	3	3	0	1
6	-0.481497	1	1	1	0	26	-0.0317791	0	3	1	1
7	0.415437	0	2	1	0	27	0.018604	1	0	2	1
8	0.0144043	0	0	0	1	28	-0.00410798	0	2	2	1
9	-0.0530054	2	0	0	1	29	-0.000606848	0	0	0	2
10	0.0143841	0	1	0	1	30	-0.0049819	1	0	0	2
11	0.0606826	1	1	0	1	31	0.0025983	2	0	0	2
12	-0.0125894	0	0	1	1	32	-0.000560528	3	0	0	2
13	0.0109689	1	0	1	1	33	-0.00163652	1	2	0	2
14	-0.133698	0	3	0	0	34	-0.000328787	1	6	0	2
15	0.00638407	0	6	0	0	35	0.000116502	2	6	0	2
16	-0.00132718	2	6	0	0	36	0.000690904	0	0	1	2
17	0.168496	3	0	1	0	37	0.00421746	0	3	1	2
18	-0.0507214	0	0	2	0	38	0.0000565229	3	6	1	2
19	0.0854559	2	0	2	0	39	-0.00146564	0	3	2	2
20	-0.0504475	3	0	2	0						

Table 5
Regression coefficient and exponent K_Q

K_Q	C	s	t	u	v	K_Q	C	s	t	u	v
		J	P/D	A_E/A_O	Z			J	P/D	A_E/A_O	Z
1	0.00379368	0	0	0	0	25	-0.0397722	0	3	2	0
2	0.00886523	2	0	0	0	26	-0.00350024	0	6	2	0
3	-0.032241	1	1	0	0	27	-0.0106854	3	0	0	1
4	0.00344778	0	2	0	0	28	0.00110903	3	3	0	1
5	-0.0408811	0	1	1	0	29	-0.000313912	0	6	0	1
6	-0.108009	1	1	1	0	30	0.0035985	3	0	1	1
7	-0.0885381	2	1	1	0	31	-0.00142121	0	6	1	1
8	0.188561	0	2	1	0	32	-0.00383637	1	0	2	1
9	-0.00370871	1	0	0	1	33	0.0126803	0	2	2	1
10	0.00513696	0	1	0	1	34	-0.00318278	2	3	2	1
11	0.0209449	1	1	0	1	35	0.00334268	0	6	2	1
12	0.00474319	2	1	0	1	36	-0.00183491	1	1	0	2
13	-0.00723408	2	0	1	1	37	0.000112451	3	2	0	2
14	0.00438388	1	1	1	1	38	-0.000029722	3	6	0	2
15	-0.0269403	0	2	1	1	39	0.000269551	1	0	1	2
16	0.0558082	3	0	1	0	40	0.00083265	2	0	1	2
17	0.0161886	0	3	1	0	41	0.00155334	0	2	1	2
18	0.00318086	1	3	1	0	42	0.000302683	0	6	1	2
19	0.015896	0	0	2	0	43	-0.0001843	0	0	2	2
20	0.0471729	1	0	2	0	44	-0.000425399	0	3	2	2
21	0.0196283	3	0	2	0	45	0.0000869243	3	3	2	3
22	-0.0502782	0	1	2	0	46	-0.0004659	0	6	2	2
23	-0.030055	3	1	2	0	47	0.0000554194	1	6	2	2

3.2 Propeller Coefficients

The characteristics of ship propellers can be denoted in non-dimensional form with the symbols (J) advance coefficient, (K_T) thrust coefficient, (K_Q) torque coefficient, and (η) efficiency. From these three coefficients, graphs can be created to help describe the performance characteristics of the propeller under various operating conditions. Observing how the K_T and K_Q curves change as the advance ratio changes makes it possible to understand how the propeller performs at various ship operational speeds and propeller rotations. Each type of ship propeller has different performance curve characteristics. Therefore, the study of ship propeller characteristics cannot be generalized to all shapes or types of propellers [21].

$$J = \frac{V_a}{nD} \tag{11}$$

$$K_T = \frac{T}{\rho\, n^2 D^4} \tag{12}$$

$$K_Q = \frac{Q}{\rho n^2 D^5} \tag{13}$$

$$\eta = \frac{JKT}{2\pi KQ} = \frac{V_a\, T}{2\,\pi\, Q\, n} \tag{14}$$

where T is propeller thrust in (N), Q is propeller torque in (Nm), ρ is Water density in (Kg/m^3), n is propeller rotation in (rad/sec), and D is Propeller diameter (m).

3.3 Polynomial B-series Propeller and CFD Simulation Results

This research's basis is using B-series propellers as the main focus. This is taken because this propeller type has fairly open access in the literature and previous research. This propeller model was chosen as the first testing step due to relevant and valid data availability. In this study, refers to Eq. (5) to Eq. (10) to calculate the propeller performance using the polynomial method. This analysis is also strengthened by considering the main dimensions of the propeller, as listed in Table 1. By combining these aspects, the performance value of the B-series propeller can be calculated. The performance results of the B-series propeller from polynomial calculations and simulations are obtained from the following data (Table 6):

Table 6
Polynomial calculation and CFD simulation results of propeller B4-40

	Polynomial method propeller B-series			CFD simulation of B-series propeller 0% camber ratio		
J	K_T	$10K_Q$	η_o	K_T	$10K_Q$	η_o
0.1	0.391	0.660	0.094	0.394	0.655	0.096
0.2	0.371	0.630	0.188	0.373	0.635	0.187
0.3	0.347	0.600	0.276	0.353	0.615	0.274
0.4	0.320	0.570	0.358	0.325	0.575	0.359
0.5	0.289	0.530	0.434	0.296	0.536	0.440
0.6	0.256	0.490	0.499	0.262	0.498	0.502
0.7	0.220	0.443	0.552	0.227	0.460	0.550
0.8	0.185	0.390	0.604	0.187	0.394	0.604
0.9	0.146	0.330	0.634	0.147	0.328	0.641
1	0.102	0.265	0.613	0.100	0.260	0.612
1.1	0.052	0.190	0.479	0.053	0.188	0.490
1.2	0.002	0.103	0.032	0.002	0.105	0.033

Table 6 and Figure 5 are presented as two sets of performance results for the propeller calculated using B-series polynomials and CFD simulations. The calculated results using B-series polynomials aim to verify and validate the results obtained from CFD simulations. In this case, the advance coefficient data (J = 0.7) was analyzed which is the performance point of the propeller. By comparing these performance results, identifying the extent of agreement and accuracy between these two analysis methods can be done.

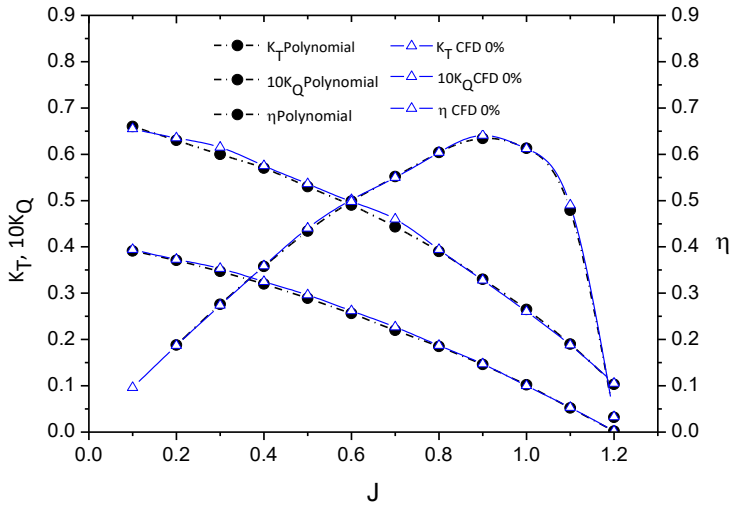

Fig. 5. Comparison of K_T, K_Q and η obtained from CFD simulation and B4-40 polynomial method for 0% camber ratio

$$J = \frac{Va}{nD} = \frac{Vs(1-w)}{\left(\frac{n}{60}\right)D} = 0.71$$

By assumtion that there is no ship in front of the propeller, so that the wake fraction value (w) is set to zero. From the above calculation the J value is 0.71. By taking J = 0.7, the analyzing propeller performance can be carried out, which resulted thrust and torque values of 37.262 N and 1.359 N/m, the thrust coefficient (K_T) and torque coefficient (K_Q) are of 0.227 and 0.046, respectively, with an efficiency value (η) in the range of 0.55.

Figure 5 shows comparison of K_T, K_Q and η obtained from CFD simulation and B4-40 polynomial method for 0% camber ratio. It can be seen, that the error difference between the polynomial calculation of the propeller and the CFD simulation for the values of K_T, K_Q, and efficiency (η) is 1.461%, 1.490%, and 0.910%, respectively. With an average error value of less than 1.5% for each propeller coefficient, it gives confidence in the effectiveness of the CFD method [22].

4. Results and Discussion

Table 7 shows the results of camber ratio variations carried out with CFD simulations. From the table, it can be seen that the measured coefficient difference values by using camber ratio are 1.6%, 2.2%, and 2.8%. From the observation simulation, at advance coefficient (J = 0.7) the average value of the thrust coefficient (K_T) increases from 1.6% to 2.2% camber ratio. However, the K_T value tends to decrease when the camber ratio is increased to 2.8%. This phenomena also occurs for the propeller's torque coefficient (K_Q) and efficiency (η).

Table 7
CFD results with camber ratio of 1.6%, 2.2%, and 2.8%

J	Camber ratio 1.6%			Camber ratio 2.2%			Camber ratio 2.8%		
	K_T	$10K_Q$	η_0	K_T	$10K_Q$	η_0	K_T	$10K_Q$	η_0
0.1	0.410	0.703	0.093	0.390	0.702	0.089	0.387	0.689	0.089
0.2	0.391	0.677	0.184	0.373	0.674	0.176	0.371	0.663	0.178
0.3	0.372	0.651	0.273	0.357	0.647	0.263	0.355	0.638	0.266
0.4	0.345	0.614	0.357	0.333	0.611	0.347	0.331	0.604	0.349
0.5	0.317	0.578	0.437	0.309	0.575	0.428	0.308	0.571	0.430
0.6	0.283	0.533	0.508	0.282	0.535	0.503	0.278	0.530	0.502
0.7	0.250	0.488	0.570	0.255	0.496	0.573	0.249	0.489	0.566
0.8	0.211	0.434	0.619	0.215	0.443	0.620	0.210	0.436	0.614
0.9	0.171	0.380	0.646	0.176	0.390	0.649	0.172	0.384	0.644
1	0.121	0.314	0.616	0.130	0.328	0.629	0.128	0.329	0.621
1.1	0.073	0.236	0.546	0.083	0.258	0.563	0.078	0.254	0.539
1.2	0.025	0.158	0.309	0.036	0.187	0.367	0.028	0.180	0.301

From the CFD simulation result, the largest efficiency value is obtained at the 2.2% camber ratio with a value of 0.573. At the same J value, (J = 0.7) the propeller efficiency increases with the value of 4.182% from 0 % to 2.2 % camber ratio as shown in Figure 6.

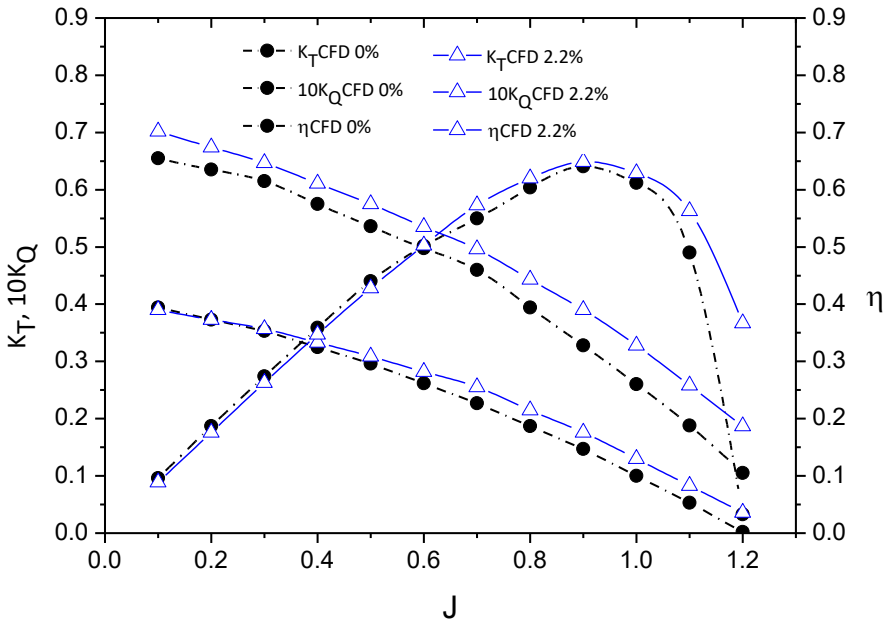

Fig. 6. Comparison of K_T, K_Q and η obtained from CFD simulation of B4-40 propeller for 0% and 2.2% camber ratio

The thrust coefficient (K_T) at each camber ratio relates to the pressure distribution in the propeller leading edge area. Pressure distribution on the propeller blade surface is illustrated in Figure 7. It can be seen that the variations in the camber ratio affect the pressure pattern on the propeller blade surface.

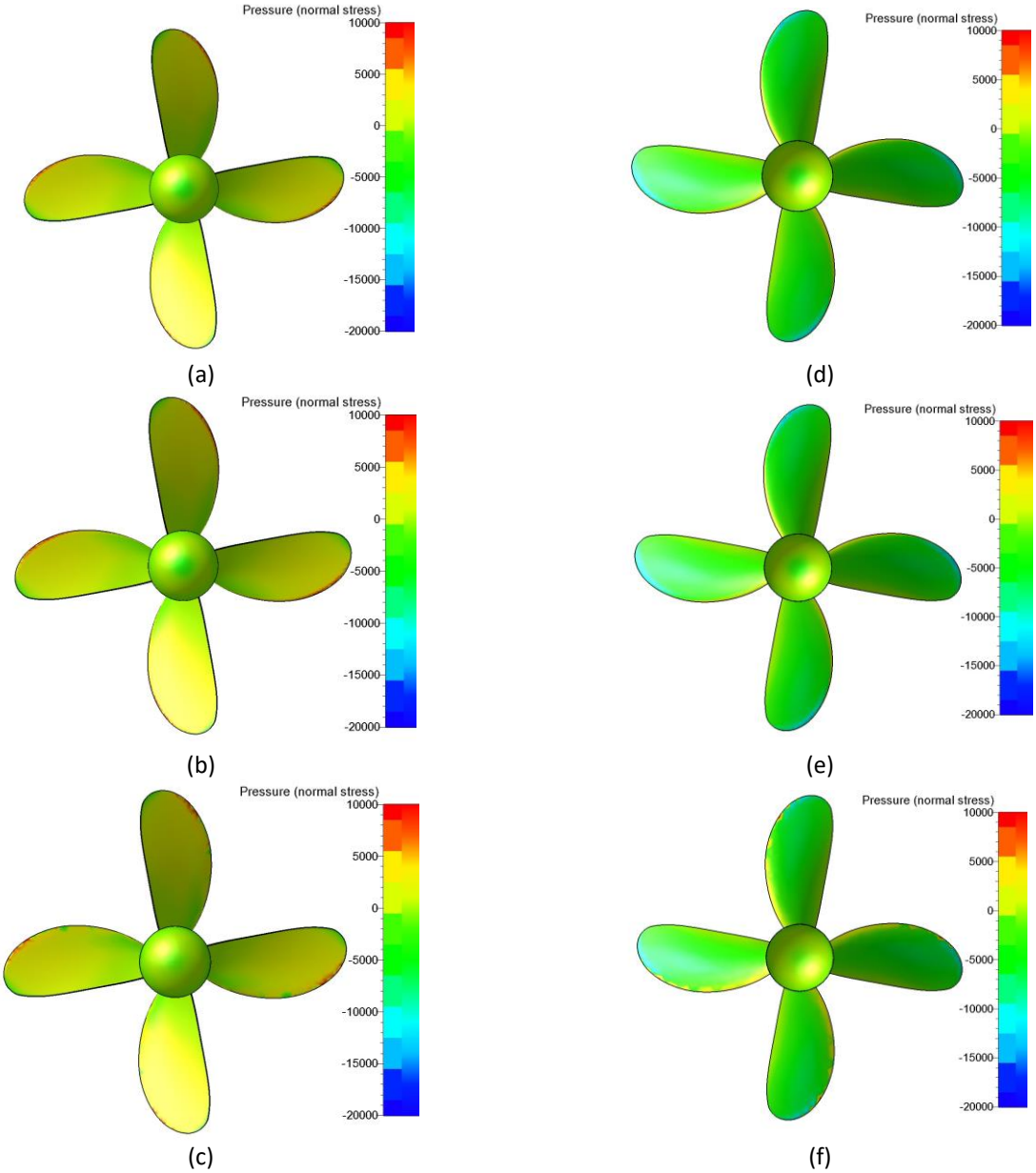

Fig. 7. Pressure distribution on the propeller blade surface at advance coefficient (J=0.7) and camber ratio variations of 1.6%, 2.2%, and 2.8%. The left column (a, b, c) shows the pressure distribution on the face side, and the right column (d, e, f) shows the back side's pressure distribution

Figure 7 shows the pressure distribution on the propeller blade surface for each camber ratio at J= 0.7. The value of 0 represents atmospheric pressure 100,000 Pascal [14], which indicates the boundary between gauge pressure and vacuum pressure.

In this analysis, the highest pressure distribution occurs around the propeller surface, especially at the leading edge from 0.6 r/R to 0.9 r/R, with the value of 110,000 Pascal (10,000 Pascal as indicated in Figure 7). This phenomenon is known as a "pressure gauge," which refers to the difference between the actual pressure measured at a point in the fluid flow and the surrounding atmospheric pressure [23].

The 2.2% camber ratio increases more pressure area (Figure 7(b)) compared to the 1.6% (Figure 7(a)) and 2.8% (Figure 7(c)). It indicates that the thrust value of camber ratio of 2.2% is slightly greater than 1.6% and 2.8%. Table 7 shows that at a camber variation of 2.2%, the advance coefficient (J=

0.7) has a slightly higher K_T value compared to the 1.6% and 2.8% camber ratio . The K_T values at J = 0.7 for each camber variation (1.6%, 2.2%, and 2.8%) are 0.250, 0.255, and 0.249, respectively.

Figure 7 (c,d,f) shows the back surface of the propeller. The pressure distribution tends to be the under atmospheric pressure with decreasing value of 5000 Pascal. This condition can be interpreted as "vacuum pressure", where the internal pressure tends to be lower than the atmospheric pressure of 1 atm (100,000 Pascal). This phenomenon occurs due to the existence of fluid flow at the back of propeller surface which absorbed and converted into propeller thrust.

5. Conclusion

This study examines the relationship between the efficiency and camber ratio variation, and this relationship is analyzed through a CFD simulation approach. The data from verifying the relationship between the B-series propeller polynomials and the CFD simulation results show that the average difference of the KT, KQ, and η coefficient values is less than 1.5%. Of the three camber ratio variations tested, the 2.2% variation showed a slightly higher average efficiency of 4.182% compared to the 1.6% and 2.8% variations. Therefore, this variation can be used as an input parameter in designing propellers for B-series displacement vessels.

This study can clarify how camber ratio variations affect propeller efficiency through a CFD simulation approach. The 2.2% camber ratio can be used as an option that results in higher efficiency and can be valuable information in designing more efficient propellers and better ship performance.

Acknowledgment

The authors gratefully acknowledge the financial support provided by the Indonesian Education Endowment Fund (LPDP) and the Ministry of Finance of the Republic of Indonesia on this research.

References

[1] Watanabe, Takayuki, Takafumi Kawamura, Yoshihisa Takekoshi, Masatsugu Maeda, and Shin Hyung Rhee. "Simulation of steady and unsteady cavitation on a marine propeller using a RANS CFD code." In *Proceedings of The Fifth International Symposium on Cavitation (Cav*. 2003.

[2] Bajuri, Muhammad Nur Arham, Djamal Hissein Didane, Mahamat Issa Boukhari, and Bukhari Manshoor. "Computational Fluid Dynamics (CFD) Analysis of Different Sizes of Savonius Rotor Wind Turbine." *Journal of Advanced Research in Applied Mechanics* 94, no. 1 (2022): 7-12. https://doi.org/10.37934/aram.94.1.712

[3] Tey, Wah Yen, Yutaka Asako, Nor Azwadi Che Sidik, and Rui Zher Goh. "Governing equations in computational fluid dynamics: Derivations and a recent review." *Progress in Energy and Environment* (2017): 1-19.

[4] Hayati, A. N., S. M. Hashemi, and M. Shams. "A study on the effect of the rake angle on the performance of marine propellers." *Proceedings of the Institution of Mechanical Engineers, Part C: Journal of Mechanical Engineering Science* 226, no. 4 (2012): 940-955. https://doi.org/10.1177/0954406211418588

[5] Wallin, Stefan. *Engineering turbulence modelling for CFD with focus on explicit algebraic Reynolds stress models*. Stockholm, Sweden: Royal Institute of Technology, Department of Mechanics, 2000.

[6] Jadmiko, Edi, Raja Oloan Saut Gurning, Muhammad Badrus Zaman, and Endang Widjiati. "Variations Rake Angle Propeller B–Series Towards Performance and Cavitation with CFD Method." *Journal of Advanced Research in Fluid Mechanics and Thermal Sciences* 106, no. 2 (2023): 78-86. https://doi.org/10.37934/arfmts.106.2.7886

[7] Suranto, Maful, I. Made Ariana, and Achmad Baidowi. "Analysis of The Effect of Pitch Angle on Propeller Modification by Considering Wake Distribution on Propeller Performance." In *IOP Conference Series: Earth and Environmental Science*, vol. 972, no. 1, p. 012049. IOP Publishing, 2022. https://doi:10.1088/1755-1315/972/1/012049

[8] Gaafary, M. M., H. S. El-Kilani, and M. M. Moustafa. "Optimum design of B-series marine propellers." *Alexandria Engineering Journal* 50, no. 1 (2011): 13-18. https://doi.org/10.1016/j.aej.2011.01.001

[9] Adietya, Berlian Arswendo, I. Ketut Aria Pria Utama, and Wasis Dwi Aryawan. "CFD Analysis into the Effect of using Propeller Boss Cap Fins (PBCF) on Open and Ducted Propellers, Case Study with Propeller B-Series and Kaplan-Series." *CFD Letters* 14, no. 4 (2022): 32-42. https://doi.org/10.37934/cfdl.14.4.3242

[10] Ariana, I. M., and B. Cahyono. "Optimization of Propeller Design Through Polynomial Approach to Optimize The Ship Energy Efficiency." In *IOP Conference Series: Earth and Environmental Science*, vol. 557, no. 1, p. 012051. IOP Publishing, 2020. https://doi:10.1088/1755-1315/557/1/012051
[11] Carlton, J. "Marine Propellers and Propulsion, 2nd edn., Buttersworth." (2007).
[12] Numeca International - Cadence Design Systems. n.d. "FINEMarine-Theory-Guide."
[13] Menter, Florian R. "Two-equation eddy-viscosity turbulence models for engineering applications." *AIAA journal* 32, no. 8 (1994): 1598-1605. https://doi.org/10.2514/3.12149
[14] Abbott, Ira H., and E. Albert. "Von Doenhoff. 1959. Theory of Wing Sections." *Dover Publications, New York* 268: 33-47.
[15] Nouri, Nowrouz Mohammad, and Saber Mohammadi. "Numerical investigation of the effects of camber ratio on the hydrodynamic performance of a marine propeller." *Ocean Engineering* 148 (2018): 632-636. https://doi.org/10.1016/j.oceaneng.2017.06.026
[16] ITTC Recommended Procedures and Guidelines. 2014. Practical Guidelines for Ship Self-Propulsion CFD. Report
[17] Abobaker, Mostafa, Sogair Addeep, Lukmon O. Afolabi, and Abdulhafid M. Elfaghi. "Effect of Mesh Type on Numerical Computation of Aerodynamic Coefficients of NACA 0012 Airfoil." *Journal of Advanced Research in Fluid Mechanics and Thermal Sciences* 87, no. 3 (2021): 31-39. https://doi.org/10.37934/arfmts.87.3.3139
[18] Molland, A. F., and I. K. A. P. Utama. "Experimental and numerical investigations into the drag characteristics of a pair of ellipsoids in close proximity." *Proceedings of the Institution of Mechanical Engineers, Part M: Journal of Engineering for the Maritime Environment* 216, no. 2 (2002): 107-115. https://doi.org/10.1243/147509002762224324
[19] Anthony F.Molland. (2011). Practical Estimation of Ship Propultion Power. Cambridge University Press, p. 32 Avenue of the Americas, New York, NY 10013-2473, USA
[20] ITTC Recommended Procedures and Guidelines. 2014. Open Water Test, Revision 3, page 3 of 11.
[21] Edward V. Lewis, Editor. (1988). Principles of Naval Architecture Second Revision, Published by The Society of Naval Architecture and Marine Engineers. 601 Pavonia Avenue, Jersey City
[22] Suastika, Ketut, Ahmad Septiawan Saputra, Adnan Faiz Fauzi, and Ahmad Firdhaus. "Comparison of Performance of Straight-and V-shaped Vanes Applied as Energy Saving Device to High-speed Boats." *CFD Letters* 15, no. 10 (2023): 110-122. https://doi.org/10.37934/cfdl.15.10.110122
[23] Versteeg, Henk Kaarle, and Weeratunge Malalasekera. *An introduction to computational fluid dynamics: the finite volume method*. Pearson education, 2007.